First Spectroscopy of the Near Drip-line Nucleus ^{40}Mg

H. L. Crawford[1*], P. Fallon[1], A. O. Macchiavelli[1], P. Doornenbal[2], N. Aoi[3], F. Browne[2], C. M. Campbell[1], S. Chen[2], R. M. Clark[1], M. L. Cortés[2], M. Cromaz[1], E. Ideguchi[3], M. D. Jones[1†], R. Kanungo[4,5], M. MacCormick[6], S. Momiyama[7], I. Murray[6], M. Niikura[7], S. Paschalis[8], M. Petri[8], H. Sakurai[2,7], M. Salathe[1], P. Schrock[9], D. Steppenbeck[9], S. Takeuchi[2,10], Y. K. Tanaka[11], R. Taniuchi[7], H. Wang[2], and K. Wimmer[7]

[1] *Nuclear Science Division, Lawrence Berkeley National Laboratory, Berkeley, CA 94720, USA*
[2] *RIKEN Nishina Center, Wako, Saitama 351-0198, Japan*
[3] *Research Center for Nuclear Physics (RCNP), Osaka University, Mihogakoa, Ibaraki, Osaka 567-0047, Japan*
[4] *Astronomy and Physics Department, Saint Mary's University, Halifax, Nova Scotia B3H 3C3, Canada*
[5] *TRIUMF, Vancouver, British Columbia V6T 2A3, Canada*
[6] *Institut de Physique Nucléaire, IN2P3-CNRS, Université Paris-Sud, Université Paris-Saclay, Orsay Cedex 91406, France*
[7] *Department of Physics, University of Tokyo, Bunkyo-ku, Tokyo 113-0033, Japan*
[8] *Department of Physics, University of York, Heslington, York YO10 5DD, UK*
[9] *Center for Nuclear Study, University of Tokyo, RIKEN Campus, Wako, Saitama 351-0198, Japan*
[10] *Department of Physics, Tokyo Institute of Technology, Meguro, Tokyo 152-8551, Japan and*
[11] *GSI Helmholtzzentrum für Schwerionenforschung GmbH, Planckstrasse 1, 64291 Darmstadt, Germany*

One of the most exotic light neutron-rich nuclei currently accessible for experimental study is ^{40}Mg, which lies at the intersection of the nucleon magic number N=28 and the neutron drip-line. Low-lying excited states of ^{40}Mg have been studied for the first time following a one-proton removal reaction from ^{41}Al, performed at RIBF RIKEN with the DALI2 γ-ray array and the Zero-Degree spectrometer. Two γ-ray transitions were observed, suggesting an excitation spectrum which shows unexpected properties compared to both the systematics along the Z=12, $N\geq$20 Mg isotopes and available state-of-the-art theoretical model predictions. A possible explanation for the observed structure involves weak-binding effects in the low-lying excitation spectrum.

The effect of weak-binding on nuclear structure, decay, and reactions is an open question in nuclear physics. On the neutron-rich side of stability, as the neutron separation energy approaches zero, weakly bound neutrons in the single-particle levels at the Fermi surface approach the edge of the nuclear potential and may move outside the core of well-bound nucleons and possibly couple to unbound continuum states. The nature of this transition from a "closed" to an "open" quantum system [1], where the binding is dominated by correlations rather than the mean field, has only just begun to be explored, and our understanding of weak-binding effects and coupling to the continuum is, in many ways, nascent.

The unexpectedly strong $B(E1)$ strength to the first excited state in ^{11}Be [2] and the strikingly large root-mean-square matter radius in ^{11}Li [3] were among the first observations suggestive of a physically extended wavefunction, now interpreted as a one-neutron $2s^1_{1/2}$ halo in ^{11}Be [4] and a two-neutron halo dominated by a $2s^2_{1/2}$ and $1p^2_{1/2}$ admixture in the case of ^{11}Li [4, 5]. Since these initial observations, more than ten nuclei have been identified as having such one- or two-neutron halo structures associated with low ℓ orbitals (ℓ=0,1) at the Fermi surface (for a complete discussion see the review articles of Refs. [4, 6, 7]).

The magnesium isotopes offer an opportunity to experimentally study the transition from well-bound to weakly-bound nuclei and its influence on excited states, which may in turn reflect the correlations at the limits of stability. While knowledge is limited in the heaviest Mg isotopes, an overall consistent picture of the structure along Z=12 has emerged between N=20 and N=28. ^{32}Mg sits at the center of the Island of Inversion [8, 9] and is understood as a prolate-deformed rotor in its ground state. Moving towards the more neutron-rich isotopes, the available spectroscopic data indicate that the Mg isotopes are prolate deformed, with assigned 2^+ and 4^+ energies consistent with quantum rotors out to ^{38}Mg (N=26), and with properties well reproduced by large-scale shell model calculations [10, 11]. A measurement of the inclusive two-proton knockout cross-section from ^{42}Si to ^{40}Mg [12] suggests that the trend for prolate deformation persists to ^{40}Mg, which was first observed as a bound system in 2007 [13]. The neighboring odd-A ^{39}Mg was confirmed as unbound, indicating the ubiquitous role of pairing correlations. The lighter odd-A ^{37}Mg is very weakly bound and has been observed to have a neutron ($2p_{3/2}$) halo component in its ground state [14, 15].

^{40}Mg represents a particularly intriguing case for study. Theoretical expectations and experimental systematics suggest ^{40}Mg to be a well-deformed prolate rotor as well, similar to ^{36,38}Mg. However, the occupation of the relatively weakly-bound $2p_{3/2}$ neutron orbital near

*Corresponding author: hlcrawford@lbl.gov
†Present address: Department of Physics and Astronomy, University of North Carolina at Chapel Hill, Chapel Hill, NC 27559-3255, USA

the Fermi surface may add a new degree of freedom not found in the lighter Mg isotopes. Specifically, the coupling of weakly bound valence neutrons to a deformed core can modify the low-energy excitation spectrum, in a manner dependent on the nature and strength of the coupling of the core and valence $2p_{3/2}$ neutrons.

In this Letter, we present the first γ-ray spectroscopic information of ^{40}Mg. We discuss the observed γ-ray transitions in the context of the systematics along the magnesium isotopes, and the potential manifestation of weak-binding effects in this exotic system.

The experiment was carried out at the Radioactive Isotope Beam Factory (RIBF), operated by the RIKEN Nishina Center and the Center for Nuclear Study of the University of Tokyo. A primary beam of ^{48}Ca, with an average intensity of 450 pnA and an energy of 345 MeV/u, was fragmented on a 2.8 g/cm^2 rotating Be production target, producing a secondary cocktail beam centered on ^{41}Al, which was selected in the first stage of the BigRIPS fragment separator [16]. Beam purification was achieved using the two-stage $B\rho-\Delta E-B\rho$ method [16], by applying a total of three magnetic rigidity selections with a 8 mm thick Al wedge degrader for energy loss located at the first momentum dispersive image, and a 5 mm thick Al wedge located at the second momentum dispersive image. The momentum acceptance for the separator was set to the maximum value of 6%.

Isotopes transported through BigRIPS to the secondary target location, in front of the ZeroDegree Spectrometer (ZeroDegree) [17], were identified event-by-event based on the $B\rho-\Delta E-$TOF method [18], with ΔE measured at the final focus using the multi-sampling ionization chamber [19]. The average secondary beam rate for ^{41}Al was 4 pps. The secondary beam cocktail delivered to the target position is shown in Fig. 1(a). The secondary beams were incident upon a polyethylene (plastic) target with thickness 3.82 g/cm^2 placed at the focal plane in front of the ZeroDegree, which was tuned to center ^{40}Mg reaction residues, and operated at the maximum momentum acceptance of 6%. Particles in the ZeroDegree were also identified on an event-by-event basis with the $B\rho-\Delta E-$TOF method. All fragments were unambiguously identified with clear separation between neighboring isotopes in A/Q and Z for the incoming beam and for reaction residues identified in the ZeroDegree as shown in Fig. 1(b).

Prompt γ rays depopulating excited states in ^{40}Mg and other reaction residues were detected in the DALI2 spectrometer [20], consisting of 186 large-volume NaI(Tl) detectors surrounding the secondary target. γ rays emitted from the fast moving nuclei ($v/c\approx 0.6$) experienced a large Doppler shift, and their energies were corrected event-by-event based on the reaction-product velocity and angle of emission of the γ ray. The Doppler correction was optimized using the known energy of the $2_1^+\rightarrow 0_1^+$ transition in ^{36}Mg [10, 21], and included an effective center-of-target offset of 2.2 cm, in agreement with the physical mid-target position.

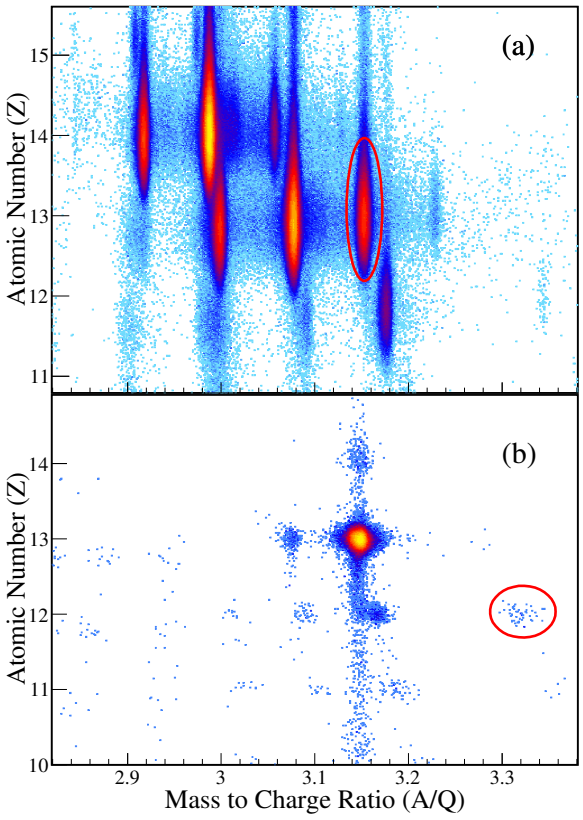

FIG. 1: (color online) Particle identification for (a) the incoming beam components as identified in the beam line detectors of BigRIPS and (b) the reaction residues following interaction of incoming ^{41}Al with the secondary target, as identified by the beam line detectors of the ZeroDegree. The ^{41}Al secondary beam is highlighted in panel (a); ^{40}Mg reaction residues are highlighted in panel (b).

The top and center panels of Fig. 2 show the prompt γ-ray spectrum observed in the DALI2 array in coincidence with incoming ^{40}Al beam particles identified in BigRIPS and with ^{36}Mg and ^{38}Mg reaction products, respectively, detected in the ZeroDegree. ^{36}Mg was produced from a -1p3n knockout/evaporation reaction and ^{38}Mg from a -1p1n knockout/evaporation. The observed transitions, at 659(6) keV and 1319(21) keV in ^{36}Mg and 635(3) MeV and 1326(14) MeV in ^{38}Mg, agree with the previously reported transitions [10, 21] assigned to the $2_1^+\rightarrow 0_1^+$ and $4_1^+\rightarrow 2_1^+$ decays, respectively. The spectra were fit between 300 keV and 3 MeV to determine the transition energies and intensities using the DALI2 response modeled in GEANT4 [22] (red dashed curves), and a double exponential decay (dotted blue line) used to model the smooth background. Below 300 keV the spectrum is dominated by atomic background induced by ions transversing the thick target; this region was not included in the fitting range. Energies were determined from the minimum χ^2 as a function of energy [23]. The observed agreement confirms both the optimization of the Doppler

correction parameters and the effective target thickness used in the analysis.

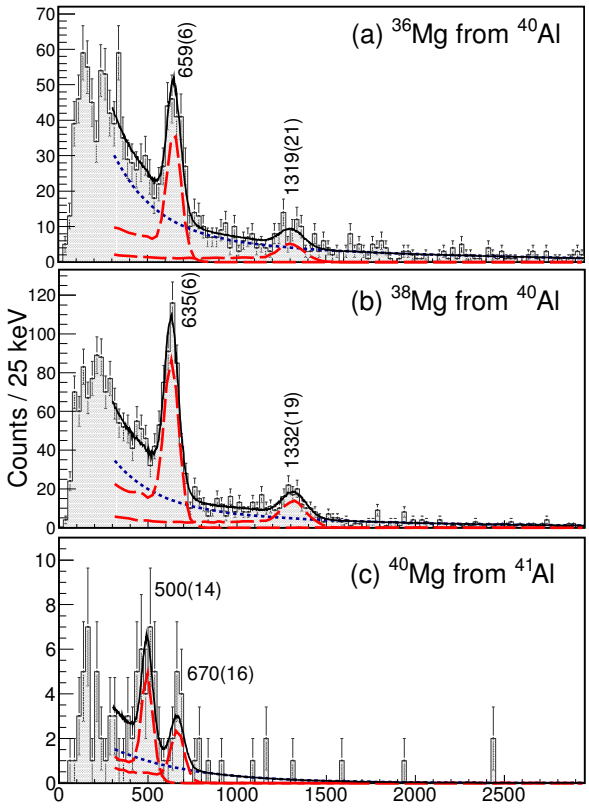

FIG. 2: (color online) Top panel: Spectrum of the prompt γ-ray transitions associated with ^{36}Mg, populated in -1p3n removal from ^{40}Al. Middle panel: Prompt γ-ray spectrum associated with ^{38}Mg, populated in -1p1n removal from ^{40}Al. Bottom panel: Prompt γ-ray spectrum associated with ^{40}Mg, populated in -1p removal from ^{41}Al. All spectra include nearest-neighbor addback and are restricted to γ-ray multiplicity ≤ 3. Spectra were fit using the DALI2 response modeled in GEANT4 (red dashed curves) and a double exponential decay (dotted blue line) used to model the smooth background; the solid black line represents the total fit.

The bottom panel of Fig. 2 (c) shows the spectrum of γ rays detected in DALI2 for an incoming ^{41}Al beam and ^{40}Mg detected in the ZeroDegree. As for ^{36,38}Mg, peak energies and intensities were obtained by fitting with simulated DALI2 peak shapes from GEANT4 to model the detector response and reaction kinematics, superposed on a fixed double-exponential background. In this case, due to the low statistics, the background shape was obtained as the average of the backgrounds obtained for ^{36,38}Mg (scaled to the number of reactions) and the freely fit background function. Two prominent low-energy peaks are observed at 500(14) and 670(16) keV, revealing a spectrum for ^{40}Mg that is very different when compared to those of ^{36}Mg and ^{38}Mg. The peaks deviate from expected statistical fluctuations in the background by 9.3σ and 4.1σ respectively. In other words, there is a less than 0.002% probability that the 670 keV peak results from background fluctuations. The structure below 300 keV is consistent within statistical fluctuations with the shape of the expected atomic background.

The γ-ray intensities were obtained by applying an absolute efficiency correction for the DALI2 array determined using the GEANT4 simulation benchmarked to γ-ray calibration sources. After correction, the 500(14) keV peak was measured to have $74(15)_{stat}(9)_{sys}$ counts, approximately 2.5 times the intensity of the 670(16) keV peak ($30(10)_{stat}(5)_{sys}$ counts). Based on its stronger population, the 500(14) keV transition is tentatively assigned as the $2_1^+ \rightarrow 0_1^+$, first excited-state to ground-state decay. The 670(16) keV transition then corresponds to the decay of a higher-energy state. However, it is unclear due to the limited statistics of the measurement whether the 500 and 670 keV transitions are in coincidence, with the higher-lying state feeding the 2_1^+.

In the scenario that the two transitions are in coincidence and form a cascade, approximately $19(7)_{stat}(3)_{sys}$% of the cross-section populates a state at 1170(21) keV, while $29(12)_{stat}(7)_{sys}$% populates the 2_1^+ state directly, with the remaining cross-section likely going to the 0_1^+ ground-state. If the two transitions are not in coincidence, then the state decaying via the 670(16) keV transition takes $19(7)_{stat}(3)_{sys}$% of the cross-section, with $48(10)_{stat}(6)_{sys}$% going to the 2_1^+ state and the remaining to the ground-state. The nature of this unexpected second transition and the low-lying state it depopulates are discussed in detail below.

We first consider the 2_1^+ state in ^{40}Mg. As shown in Fig. 3, shell-model calculations using the SDPF-MU [24] and SDPF-U [11] interactions predict a flat trend in $E(2_1^+)$ and $E(4_1^+)$ all the way to ^{40}Mg, after decreasing slightly from the higher excitation energies at ^{32}Mg. The trend for similarly deformed ground states from ^{32}Mg out to ^{40}Mg is consistently obtained in many other calculations [25–28] and overall these calculations agree very well with the known data up to ^{38}Mg. The trend predicted within the shell-model for a 2_1^+ energy in the range of 650-700 keV for ^{40}Mg is in contrast with the $E(2_1^+)$ observed in the current work, where the energy of 500(14) keV shows a $\sim$20% decrease relative to ^{38}Mg. Recognizing that relative changes in energy are perhaps a more robust prediction than the absolute values, it is important to note that the decrease in the 2_1^+ energy at ^{40}Mg and the overall trend along the Mg isotopes is not reproduced in any currently published calculation [11, 24–28].

The observation of a second low-energy transition at 670(16) keV in ^{40}Mg, and hence a likely second state below 1.2 MeV, is even further outside of current model predictions and experimental systematics. Based on the trend of final states populated in the one-proton removal reactions into ^{36,38}Mg, one would expect to populate (if bound) the 4_1^+ state at about 2 MeV and to observe a de-populating γ-ray transition to the 2_1^+ state at approx-

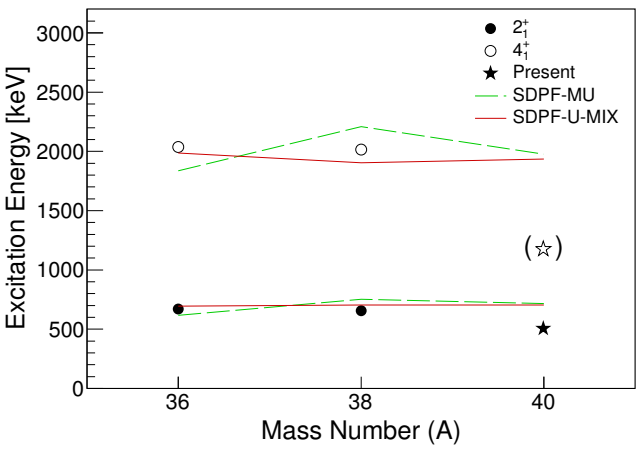

FIG. 3: (color online) Known experimental E(2_1^+) (filled symbols) and E(4_1^+) (open symbols) energies for ^{36}Mg and ^{38}Mg [10, 21]. Also included is the E(2_1^+) for ^{40}Mg inferred here (filled star). The open star indicates the energy of the second excited state in ^{40}Mg under the assumption that the two observed γ-ray transitions form a cascade (see text for details). The data are compared to shell-model calculations using the SDPF-MU [24] and SDPF-U-MIX [11] effective interactions.

imately 1.3 MeV. No calculation predicts a 4_1^+ state only 670 keV above the 2_1^+ state giving a very low $R_{4/2}$ ratio of only 2.34.

Alternatively, shell model and mean-field calculations predict ^{40}Mg to have a coexisting oblate-deformed configuration at relatively low excitation energy, with a 0_2^+ oblate state at $\geq$1.5 MeV excitation energy, though in most calculations it is well above 2 MeV. It is possible that the 670 keV transition could be associated with states in the oblate configuration. This scenario, however, is not supported by a previous cross-section analysis, where the inclusive two-proton removal cross-section from ^{42}Si to ^{40}Mg was observed to be very small, only 40^{+27}_{-17} μb [12]. This cross-section was shown to be consistent with only one of the predicted coexisting shapes being bound – most likely the prolate shape – with the oblate 0_2^+ then being above the neutron separation energy [12].

Another possibility for the second observed state is a 2_2^+ level that decays to the 2_1^+, which may occur in the presence of a strong axially-asymmetric deformation. In this case, the observed level energy ratio E(2_2^+)/E(2_1^+) would imply a triaxial deformation of γ=25.4$^{+0.6}_{-0.5}$ degrees [29], close to the maximum of γ=30 degrees. Once again, this is outside the predictions of all published calculations, which describe the nucleus as dominated by axially-symmetric quadrupole deformation and prolate-oblate shape coexistence with little mixing. We note that, for $\gamma \approx 25$ degrees, the decay from the 2_2^+ directly to the ground state is expected to have a similar transition strength as the $2_2^+ \rightarrow 2_1^+$ transition, leading to a γ-ray transition at 1170(21) keV with 5(2) counts in our spectrum, which cannot be ruled out within the experimental uncertainties.

It is clear that the observed spectrum of ^{40}Mg does not follow the systematics expected from either data, or predicted by theory, including the large-scale shell-model calculations which have proven so successful in describing both the lighter Mg isotopes and the heavier N=28 isotones (^{42}Si and ^{44}S). However, ^{40}Mg is near the limits of binding with a model-extrapolated one-neutron separation energy (S_n) value of 2.0(7) MeV [30] and, according to Nilsson and shell model calculations [11, 31], likely has two neutrons in the low-ℓ $2p_{3/2}$ orbital at the Fermi surface, giving rise to the potential for an extended neutron wavefunction. In this case, we may consider ^{40}Mg as a deformed ^{38}Mg, surrounded by an extended two-neutron p-wave halo, a picture consistent with recent Hartree-Fock-Bogolyubov calculations [32]. It is of interest then to ask the question: might the observed γ-ray spectrum and breakdown of systematics at ^{40}Mg be the result of weak-binding effects not captured in the current calculations?

We consider two simplified scenarios to describe the coupling of the weakly-bound $2p_{3/2}$ neutrons to the core. The first assumes that it is possible to generate 2^+ excitations from the core rotation and by recoupling the valence neutrons to a $p^2_{3/2}$ 2^+ configuration, and that these two degrees of freedom are weakly coupled. If the energy required to recouple the valence neutrons is of order the core 2^+ energy, then the resultant two 2^+ states can be highly mixed, giving rise to two low-energy transitions, as observed, where both 2^+ levels directly feed the ground state. In fact, a simple volume scaling [33] of the two-body matrix element for the 2^+ $\nu 2p^2_{3/2}$ configuration on top of ^{50}Ca ($\simeq$1 MeV) results in a $2p^2_{3/2}$neutron 2_1^+ energy of $\simeq$550 keV for ^{40}Mg, close to the core $E_{2_1^+}$. Alternatively, if the $2p_{3/2}$ neutrons follow the core deformation, as suggested in Ref. [32], then it is possible to generate a paired rotational band based on the ground state (with properties similar to ^{38}Mg) and an aligned rotational band, where the angular momenta of the $2p_{3/2}$ neutrons (j=2) are aligned to the rotational core angular momentum due to the Coriolis force [34]. Since it is possible that the reduced spatial overlap between the extended $\nu 2p_{3/2}$ halo with the core will weaken the pair correlations, consistent with the description of HFB calculations [32], the excitation energy of the aligned band in ^{40}Mg will be lowered relative to that expected for ^{38}Mg. In this scenario, a pairing gap of $\sim$500 keV will result in a 2_2^+ state from the aligned band close to the 2_1^+ of the ground-state band, a similar picture to the one above. It is also worth noting that in either description we also expect a lowered 4_1^+ state, which if bound could be populated. However, based on the relative population of the 2_1^+ and 4_1^+ state in the proton removal reactions into ^{36,38}Mg [10] and the present statistics, it is not clear that we would expect to see the associated γ-ray transition(s).

The above qualitative discussions indicate that weak-

binding effects could produce a spectrum of excited states consistent with that observed in ^{40}Mg, and would signal a departure from the structural characteristics of well-bound nuclei. However, more fully microscopic models taking into account extended wavefunctions and coupling to the continuum, such as those adopted in Ref. [28, 35] for example, are required to provide a quantitative description and to fully explore the impacts of weak binding on the collective and single-particle excitation modes.

In summary, γ-ray transitions have been observed in ^{40}Mg for the first time in a one-proton removal reaction from ^{41}Al, studied at RIBF RIKEN, using the ZeroDegree and DALI2. The observed spectrum, with two transitions at 500(14) and 670(16) keV, is strikingly different from the neighboring ^{36,38}Mg. The tentatively assigned $2^+_1 \rightarrow 0^+_1$ transition at 500(14) keV is 20% below that in ^{38}Mg, a trend which is outside of shell-model and other state-of-the-art theoretical predictions. The second γ-ray transition is even more puzzling. While most models would favor this transition as associated with a coexisting configuration (shape), there are currently no model predictions for a second low-lying (below $\sim$1.5 MeV) state in ^{40}Mg consistent with our observation. However, given that ^{40}Mg is very near the neutron dripline, and the low-ℓ $\nu 2p_{3/2}$ orbital sits at the Fermi surface, the observed spectrum may be an indication for the manifestation of weak-binding effects. We have speculated on possible scenarios, but more detailed calculations are required for the structure of ^{40}Mg and other weakly-bound systems which may become accessible in the future, as next generation radioactive beam facilities come on-line.

Acknowledgements We thank the accelerator operations staff at RIBF/RIKEN Nishina Center for their outstanding work in primary beam delivery, and the BigRIPS team for preparing the secondary beam. We also thank GSI for the MUSIC ionization chambers used for particle identification in the ZeroDegree. This work was supported by the U.S. Department of Energy under Contract No. DE-AC02-05CH11231 (LBNL) and by the Royal Society under contract number UF150476 and the U.K. STFC under contract number ST/L005727/1.

[1] J. Dobaczewski, N. Michel, W. Nazarewicz, M Ploszajczak and J. Rotureau, Prog. Part. Nucl. Phys. **59**, 432 (2007).
[2] S. S. Hanna, K. Nagatani, W. R. Harris and J. W. Olness, Phys. Rev. C **3**, 2198 (1971).
[3] I. Tanihata, H. Hamagaki, O. Hashimoto, Y. Shida, N. Yoshikawa, K. Sugimoto, O. Yamakawa, T. Kobayashi and N. Takahashi, Phys. Rev. Lett. **55**, 2676 (1985).
[4] I. Tanihata, H. Savajols and R. Kanungo, Prog. Part. Nucl. Phys. **68**, 215 (2013), and references therein.
[5] P. G. Hansen and B. Jonson, Europhys. Lett. **4**, 409 (1987).
[6] T. Nakamura, H. Sakurai and H. Watanabe, Prog. Part. Nucl. Phys. **97**, 53 (2017), and references therein.
[7] T. Aumann and T. Nakamura, Phys. Scr. **T152**, 014012 (2013), and references therein.
[8] A. Poves and J. Retamosa, Phys. Lett. **B184**, 311 (1987).
[9] E. K. Warburton, J. A. Becker and B. A. Brown, Phys. Rev. C **41**, 1147 (1990).
[10] P. Doornenbal, H. Scheit, S. Takeuchi, N. Aoi, K. Li, M. Matsushita, D. Steppenbeck, H. Wang, H. Baba, H. Crawford *et al.*, Phys. Rev. Lett. **111**, 212502 (2013).
[11] E. Caurier, F. Nowacki and A. Poves, Phys. Rev. C **90**, 014302 (2014).
[12] H. L. Crawford, P. Fallon, A. O. Macchiavelli, R. M. Clark, B. A. Brown, J. A. Tostevin, D. Bazin, N. Aoi, P. Doornenbal, M. Matsushita *et al.*, Phys. Rev. C **89**, 041303 (2014).
[13] T. Baumann, A. M. Amthor, D. Bazin, B. A. Brown, C. M. Folden III, A. Gade, T. N. Ginter, M. Hausmann, M. Matos, D. J. Morrissey *et al.*, Nature **449**, 1022 (2007).
[14] M. Takechi, S. Suzuki, D. Nishimura, M. Fukuda, T. Ohtsubo, M. Nagashima, T. Suzuki, T. Yamaguchi, A. Ozawa, T. Moriguchi *et al.*, Phys. Rev. C **90**, 061305(R) (2014).
[15] N. Kobayashi, T. Nakamura, Y. Kondo, J. A. Tostevin, Y. Utsuno, N. Aoi, H. Baba, R. Barthelemy, M. A. Famiano, N. Fukuda *et al.*, Phys. Rev. Lett. **112**, 242501 (2014).
[16] T. Kubo, D. Kameda, H. Suzuki, N. Fukuda, H. Takeda, Y. Yanagisawa, M. Ohtake, K. Kusaka, K. Yoshida, N. Inabe *et al.*, Prog. Theor. Exp. Phys. **2012**, 03C003 (2012).
[17] Y. Mizoi, T. Kubo, H. Sakurai, K. Kusaka, K. Yoshida and A. Yoshida, RIKEN Accelerator Progress Report **38**, 297 (2005).
[18] N. Fukuda, T. Kubo, T. Ohnishi, N. Inabe, H. Takeda, D. Kameda and H. Suzuki, Nucl. Instrum. Methods Phys. Res. B **317**, 323 (2013).
[19] R. Schneider and A. Stolz. Technical Manual Ionisation Chamber MUSIC80. Retrieved from: `https://www-win.gsi.de/frs/technical/FRSsetup/detectors/music80/music80\_manual.pdf`
[20] S. Takeuchi, T. Motobayashi, Y. Togano, M. Matsushita, N. Aoi, K. Demichi, H. Hasegawa, and H. Murakami, Nucl. Instrum. Methods Phys. Res. A **763**, 596 (2014).
[21] A. Gade, P. Adrich, D. Bazin, M. D. Bowen, B. A. Brown, C. M. Campbell, J. M. Cook, S. Ettenauer, T. Glasmacher, K. W. Kemper, S. McDaniel, *et al.*, Phys. Rev. Lett. **99**, 072502 (2007).
[22] S. Agostinelli, J. Allison, K. Amako, J. Apostolakis, H. Araujo, P. Arce, M. Asai, D. Axen, S. Banerjee, G. Barrand *et al*, Nucl. Instrum. Methods Phys. Res. A **506**, 250 (2003).
[23] S. Baker and R. D. Cousins, Nucl. Instrum. Methods Phys. Res. **221**, 437 (1984).
[24] Y. Utsuno, T. Otsuka, B. A. Brown, M. Honma, T. Mizusaki and N. Shimizu, Phys. Rev. C **86**, 051301(R) (2012).
[25] M. Shimada, S. Watanabe, S. Tagami, T. Matsumoto, Y. R. Shimizu and M. Yahiro, Phys. Rev. C **93**, 064314 (2016).
[26] T. Rodríguez, Eur. Phys. J. A **52**, 190 (2016).

[27] M. Kimura, T. Suhara and Y. Kanada-En'yo, Eur. Phys. J. A **52**, 373 (2016).
[28] K. Fossez, J. Rotureau, N. Michel, Q. Liu and W. Nazarewicz, Phys. Rev. C **94**, 054302 (2016).
[29] A. S. Davydov and G. F. Filippov, Nucl. Phys. **8**, 237 (1958).
[30] M. Wang, G. Audi, F. G. Kondev, W. J. Huang, S. Naimi and X. Xu, Chinese Phys. C **41**, 03003 (2017).
[31] I. Hamamoto, Phys. Rev. C **93**, 054328 (2016).
[32] H. Nakada and K. Takayama, Phys. Rev. C **98**, 011301(R) (2018).
[33] W. W. Daehnick, Physics Reports **96**, 317 (1983).
[34] F. S. Stephens and R. S. Simon, Nucl. Phys. A **183**, 257 (1972).
[35] H.-W. Hammer, C. Ji and D. R. Phillips, J. Phys. G: Nucl. Part. Phys. **44**, 103002 (2017).